The Sunairio Method for Solar Production Risk Assessment

Brent Ho+, Eric Hewitt+, Olivia Pfeiffer+, Tim Ivancic+, Barry L. Nelson*, and Rob Cirincione+

+*Sunairio Inc., Baltimore, MD, 21202, USA*
**Department of Industrial Engineering and Management Sciences, Northwestern University, Evanston, IL, 60208, USA*

August 2023

Abstract

Solar production risk assessment is traditionally based on hypothetical power generation calculated from Typical Meteorological Years (TMYs) or historical weather data. These approaches ignore climate trends and extrapolate from small datasets, leading to production estimates that are unreliable and drift from reality over time. Sunairio addresses these shortcomings via a system of stochastic climate simulations to create arbitrary amounts of realistic local-climate-adjusted weather data.

On 100 representative US solar sites, we first verified that the Sunairio simulation method generated realistic weather. We then found TMYs to be unrepresentative and to overpredict power generation at 85% of the sites. We found site-dependent local-climate-trend production adjustments to range from -6.16% to 2.77% of predicted production in 2022 — adjustments that grew in magnitude to -13.48% to 4.63% when extrapolated out to 2034. An overall negative GHI trend of -0.225 W/m^2 per year (83% of the sites had negative GHI trends) caused overall production losses of 2.43% in 2022 and 4.98% in 2034 with respect to TMY estimates. Finally, the degree of uncertainty in production estimates was at least four times lower in the Sunairio simulation data compared to production estimates using historical samples.

1 Introduction

1.1 Motivation

Solar production risk assessment is a difficult task for solar project developers and investors, who need to understand the impact of production volatility on financial risk metrics. To assess the financial and practical viability of potential solar sites, analysts typically rely on hypothetical power production predictions which are based on historical weather data. However, such projections are unreliable, as there is insufficient data to smooth out year-to-year variance — and no single year can be taken as representative.

In this introductory section, we

- Introduce the current approaches to solar production risk assessment (Section 1.2).
- Document their manifest limitations (Section 1.3).
- Present a new alternative solar production estimation method (Section 1.4).
- Outline a study that compares the relative fidelity and accuracy of all three approaches (Section 1.5).

1.2 Current approaches

1.2.1 Typical Meteorological Years

The first (and still most common) tool for solar production risk assessment is the hypothetical "Typical Meteorological Year" (TMY), introduced by the Sandia National Laboratories in 1978 [1]. Under this selection and concatenation paradigm, twelve "representative" months of weather (one for each calendar month) are selected from a location's historical data. The twelve months, which typically come from different calendar years, are then simply concatenated together to create a TMY.

This paradigm, which was dependent on heuristics and for which "[n]o extensive validation has been performed to assess the typicality of the years generated" [1], has since become widespread in the solar industry. TMYs created with a variety of slightly different selection algorithms[1] are now available for locations across the United States.

1.2.2 Historical time series

Another method of solar production risk assessment is to simply evaluate power production numbers using historical data. Although not often explicitly stated, this approach considers historical weather as samples of the "true" weather distribution — and takes sample statistics (means, medians, exceedance values, etc.) as empirical estimates of true values.

[1]Most notably SolarGIS [2] and TMY3 [3].

1.3 Limitation of current approaches

To properly evaluate a potential solar site, one first needs robust estimates of expected future power generation. Given weather variability and the resulting variability in power generation, one also needs to account for the shape and spread of the future power generation distribution.

As we shall see, TMYs are not typical years of meteorological data. More impactfully for solar power risk assessment, they also **consistently overpredict irradiance and power generation**. And as TMYs are point estimates of annual irradiance and generation distributions they provide no measure of variability — and are thus of limited use in determining risk.

Power estimates derived from yearly historical means, on the other hand, can provide some measurement of variability. Given n years of historical weather data, one has created n years of hypothetical generation data. Ideally, the distribution and mean of these points would be precise and unbiased representations of the true power distribution.

Unfortunately, this is not the case. Historical estimates have low precision due to a paucity of data. While temperature data are available for many decades[2], local irradiance data are a relatively recent phenomenon, with the widely used National Solar Radiation Database (NSRDB) [5], for example, only providing data since 1998. Point estimates from these empirical distributions (which therefore contain at most 25 annual points) are at best noisy approximations of their true counterparts. In fact, we will find a 0.93% uncertainty in annual mean generation predictions due to the large variance and small historical sample size.

More damaging to solar power predictions than the issue of preciseness, however, is the question of bias — particularly with respect to local climate trends in temperature and irradiance. TMY algorithms and historical time series analysis are idealized as representative or unbiased estimates of a *stationary* weather distribution (one that does not change over time) — which is demonstrably false. As a result, predictions of the present are biased because they do not account for the trend, and these biases only increase in magnitude as one predicts dates further into the future. We will find local climate trends to have a profound influence on solar site potential.

As an example, Figure 1 depicts annual temperature averages and a fitted linear trend on a selected solar site. The average temperature from TMY and Historical weather data (which underpredict with respect to current and future years) are shown as horizontal lines.

[2]In the case of the Central England Temperature dataset[4], several centuries

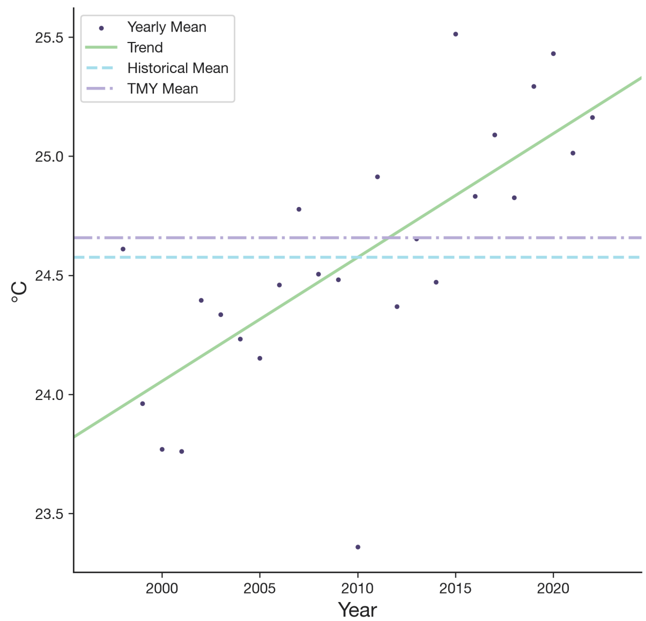

Figure 1: Annual temperatures *at the Miami-Dade Solar Energy Center displaying significant year-to-year variance, a positive trend, and TMY (historical) estimates that ignore the trend and approximate the median (mean) of the distribution.*

1.4 Stochastic climate simulation for solar production risk assessment

The Sunairio method attempts to account for the aforementioned issues of bias and precision via a system of stochastic simulation.

In the Sunairio system, historical data are seen as trended samples from an underlying site-specific weather distribution. Climate trends in temperature and Global Horizontal Irradiance (GHI) are calculated and used to detrend historical data. The resulting data are then used to create weather distributions for all hours of a calendar year, which are sampled (with adjustments to maintain site-to-site correlations and autocorrelation structure) to create weather simulations which can be extended arbitrarily into the future. Solar generation is modeled on the simulation weather and analyzed.

Through this system, one can create a large amount[3] of simulation data at hourly temporal resolution.[4] By design, each simulation path is independent of all other paths and all paths are explicitly adjusted for local trends in weather. Large amounts of data decreases noise in power generation estimates; grounding simulations in *detrended* historical data reduces bias and susceptibility to climate trends.

[3]We typically create 1000 simulation paths.

[4]It is important to model weather at high temporal resolution (as opposed to annually) due to seasonal, intraday, and inverter effects on solar power generation. In fact, resolution higher than hourly could even lead to better results [6].

1.5 The study

In this study, we analyzed the effect of analysis method (TMY, historical time series, or stochastic climate simulation) on weather and predicted solar production.

We first selected 100 solar sites across the continental US. Using 25 years of detrended historical weather data, we then created 1000 simulation paths for each site and compared GHI and modeled generation numbers for weather based on TMYs, historical data, and simulations (SIM-2022).

As the value of the simulation data is largely dependent on the ability of the stochastic simulations to reproduce and extend patterns and trends from historical weather data, we also created simulations (SIM-RAW) based on raw historical (as opposed to detrended historical) weather data. We confirmed, via analysis of GHI and power predictions, that these simulations did not deviate from historical data.

To demonstrate the ramifications of the method's ability to extend weather predictions far into the future, we also created and analyzed stochastic simulations with climate trends extended to 2034 (SIM-2034).[5]

In all, there were 5 weather datasets that we considered for each solar site:

1. TMY: 1 "year" of TMY data
2. HIST: 25 years of historical data
3. SIM-RAW: 1000 simulation runs from raw historical data
4. SIM-2022: 1000 simulation runs from detrended historical data
5. SIM-2034: 1000 simulation runs from detrended historical data, extended to 2034

2 Methods

In the sections below we discuss the following:

1. Solar site selection (Section 2.1).
2. Weather data sources (Section 2.2).
3. The TMY algorithm (Section 2.3).
4. Climate trends (Section 2.4).
5. Stochastic climate simulation (Section 2.5).
6. Solar power modeling (Section 2.6).

2.1 Solar site selection

We wanted to select a representative sample of US utility-scale projects. To this end, we selected 100 solar sites from the US Energy Information Administration's (EIA) Form 860 database of electric generators [7]. 50 sites had

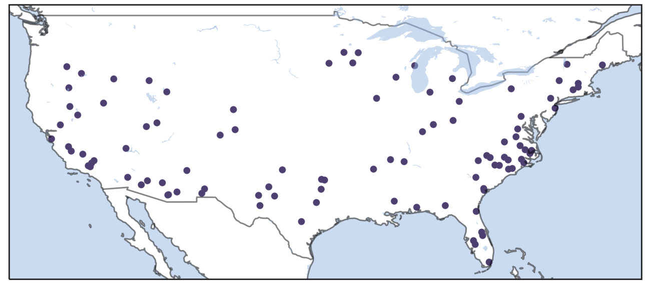

Figure 2: Selected solar sites, *chosen to cover a range of geographies and technical configurations.*

nameplate capacities between 5MW and 20MW, while the remaining 50 sites had nameplate capacities above 50MW.

We selected sites that were well distributed in latitude, longitude, and DC/AC ratios[6]. The selected generators covered a large range of technical configurations, DC/AC ratios between 1.00 and 1.88, installation years between 2010 and 2021, and nameplate capacities between 5MW and 240MW. The geographic distribution of the selected generators is shown in Figure 2.

2.2 Weather data sources

Data for this study were provided by a combination of sources. Temperature readings came from ERA5 and were downscaled using elevation data from the Global Land One-kilometer Base Elevation (GLOBE) dataset. Irradiance data came from a dataset made using a combination of the National Solar Radiation Database (NSRDB), Geostationary Operational Environment Satellite (GOES) data, and the High Resolution Rapid Refresh model (HRRR) — all bias-corrected against the Baseline Solar Radiation Network (BSRN).

All weather data inputs were downscaled and interpolated to the centroids of the analyzed sites, giving us 25 years of complete hyper-local weather data (1998-2022).[7]

2.3 TMY generation

As the latest TMYs provided by NREL/Sandia [8] are only available at 4km resolution and only considered weather data from 1998-2017, we re-implemented the most recent TMY algorithm (TMY3) to create TMYs at each of our solar sites.

As with all TMY algorithms, the TMY3 algorithm [3] selects 12 "representative" calendar months — one representative January, one representative February, etc. — and concatenates their respective weather together to

[5]As we focused on the effect of different weather sources on predictions, we did not explicitly model solar cell degradation over time, although correcting for this would not affect our results significantly.

[6]We chose a spread of DC/AC ratios to control for inverter clipping effects.

[7]Temperature data are available since 1950; irradiance data are available since 1998.

form a "typical" year. With 25 years of historical data, candidate months from 25 different years can be selected to represent each calendar month in the TMY.

Months are selected in a 3 step process (more details can be found in Appendix A):

(i) Choose 5 candidates via weighted Finkelstein-Schafer statistics.
(ii) Discard candidates due to persistence criteria.
(iii) Select the top candidate by proximity to long-term means and medians.

The selected months are then combined to make the TMY at that site.

2.4 Climate trends

Given the small number of historical years and considerable noise in weather averages, we used linear regression models on yearly averages to calculate climate trends for each weather variable at each location. The simulation model framework, however, is also compatible with physics-based climate models.[8] Figure 3 depicts the sign and magnitude of temperature and GHI trends for the selected sites.[9]

Temperature trends were positive for all 100 sites with a mean trend of 0.030 °C/yr — consistent with the 0.027 °C/yr rise in North America found in [11]. Detected trends ranged between 0.021 °C/yr and 0.047 °C/yr.

More importantly for solar production assessment, **GHI trends were negative for 83 of the 100 sites**, with a mean trend of $-0.225 W/m^2$/yr. Detected trends ranged between $-0.640 W/m^2$/yr and $0.314 W/m^2$/yr and varied regionally — with positive trends in the Western US and negative trends elsewhere, particularly in the Midwest.

Global Climate Models have difficulty resolving cloud dynamics due to the localized nature of convective cells. As such there is little consensus on the trend in GHI from climate researchers. However, we feel that trends in precipitation may serve as a proxy for cloud cover and thus have an inverse relationship with GHI. In fact, precipitation trends show good agreement with our observations of GHI. The Fourth National Climate Assessment [12] reports a pronounced trend in annual precipitation in both observations and climate models with positive trends in the Eastern US and negative trends in the Western US.

2.5 Stochastic climate simulation

To create weather simulations, we first computed Cumulative Distribution Functions (CDFs) for each weather variable and each hour of the year.

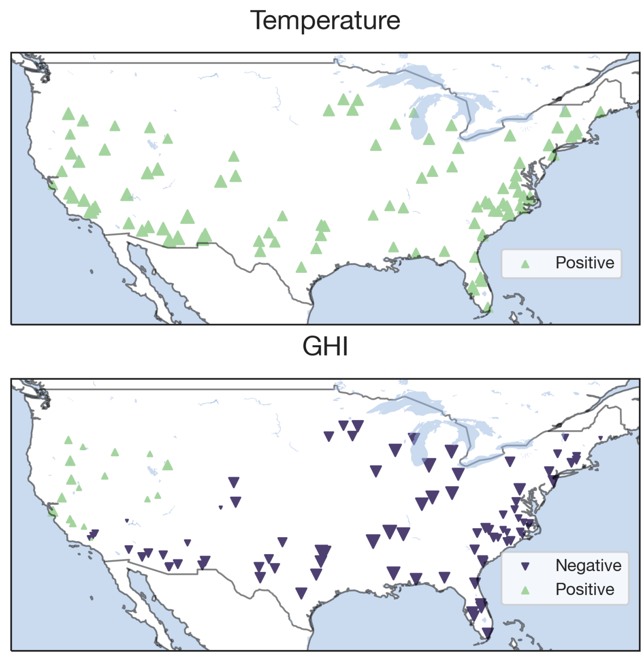

Figure 3: Local climate trends *calculated at the selected solar sites. Color and icon direction indicate trend direction; icon size indicates trend magnitude. We note positive temperature trends and regional but broadly negative GHI trends.*

For SIM-RAW, CDFs were computed on unadjusted historical data; for SIM-2022 and SIM-2034, CDFs were computed on historical data detrended to year y.

For example, if we detected a positive temperature trend at a location and were detrending to the year 2022 (SIM-2022), we adjusted hourly weather readings upward (Figure 4 shows the magnitude of detrending adjustments per year). Hourly adjustments were refined to satisfy various physical requirements.[10]

These distributions were then used to sample, with adjustments to maintain historical correlation and autocorrelation structure across time, solar sites, and weather variables. Maintenance of these correlation structures ensures realistic regional weather predictions and effectively increases site training data size.

For each simulation setup (SIM-RAW, SIM-2022, and SIM-2034), we created 1000 hourly year-long paths for all solar locations and variables.

2.6 Solar power model

While some PV solar production models, such as NREL's physics-based PVWatts [13], can model solar production using a comparatively small set of inputs, these models utilize empirically-derived algorithms — making

[8] Current climate models do not accurately predict clouds — and hence GHI ([9], [10])

[9] While linear trends are appropriate for shorter time horizons (e.g. in this study), trends over longer time horizons may stray from linear patterns according to socio-economic pathways and government actions.

[10] No negative irradiance numbers, irradiance adjustments only during daylight hours, etc.

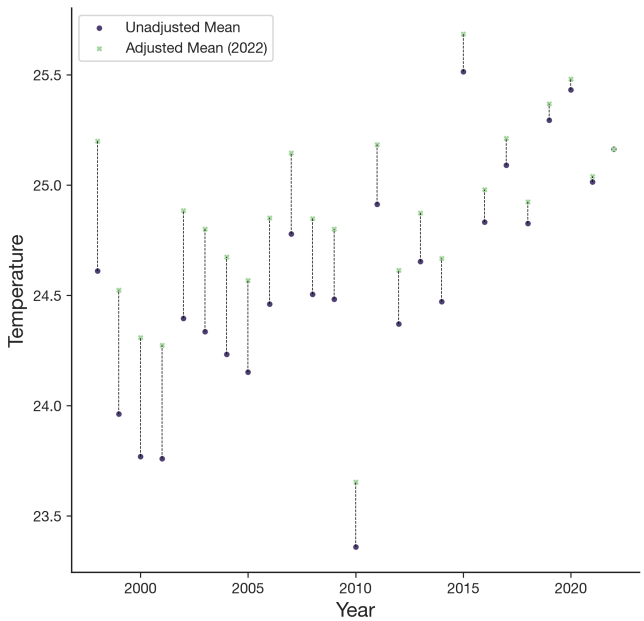

Figure 4: Adjustments to detrend temperature *at the Miami-Dade Solar Energy Center into 2022-equivalent temperatures. Adjustments decrease in magnitude as the historical year approaches the target year of 2022.*

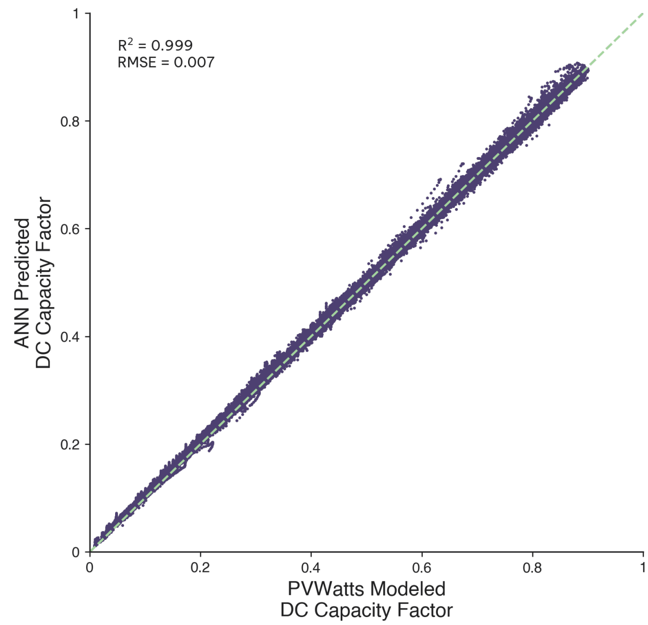

Figure 5: Validation of solar model production predictions *by comparing model predictions (y-axis) to NREL's PVWatts predictions (x-axis) at noon hours on 16 solar sites (n=1,789,632).*

them slow to run on simulations of many sites over long time horizons. The machine-learning-based Sunairio Solar Power Model, on the other hand, makes reliable predictions from a simple set of inputs — with a runtime low enough to enable large-scale applications.

The Sunairio Solar Power Model was constructed using Artificial Neural Nets (ANNs) on twelve features. Four of the features (solar zenith angle, solar azimuth angle, GHI, and temperature) change hour-by-hour; eight features describe the installed capacity and configuration of the solar site (see Table 1). This set includes just two weather variables as a deliberate design choice to limit data overhead and model complexity.[11]

The non-linear nature of solar power makes ANNs quite suitable for capturing the complex relationship between weather, orientation angles, and power output.

We trained our ANN on 717 hypothetical solar sites (varying location, technical characteristics, and weather) to replicate power production predictions generated from `pvlib-python`'s implementation of PVWatts.[14]

Validation against physics models We validated our solar power model on 16 solar sites by comparing model ANN solar power predictions against production estimates from physics-based industry-standard models. The mean R^2 was 0.98. Figure 5 shows physics-based models against model predictions at noon hours, where R^2 was 0.999.

We validated further by comparing ANN solar power model predictions to PVWatts modeled power at all 48 state capitals in the contiguous United States. We evaluated two technical configurations: A) 250 MW fixed-tilt and B) 250 MW single-axis tracking. The mean percent differences across all sites were 0.309% and 0.296%, respectively. Tables with all annual generation values for both PVWatts and the ANN can be found in Appendix B.

3 Stochastic climate simulation validation

To verify that our simulation methods produce realistic data, we first created 1000 simulation runs (each containing a year of data) for each of the 100 sites without any climate trend corrections. The simulation results should have similar weather and generation distributions as historical data — but lots more data.[12] (Section 3.1)

We then verified that our climate trend adjustments worked as expected (Section 3.2).

[11] For example, while other models relied on explicit decomposition GHI into DNI and DHI components as data inputs, the Sunairio model learned this decomposition implicitly.

[12] 1000 samples of simulated meteorological years as opposed to 25 years of historical data.

	Description
Site Coordinates	Latitude and longitude of solar site
DC Capacity	Installed DC panel capacity
Albedo	Ground reflected fraction of incident sunlight
GCR	Ratio of solar array area to total ground area
Bifacial Gain	Generation gained due to bifaciality
Tilt Angle	Angle of panels from the horizontal
Tracking Type	Tracking strategy: fixed or single-axis
Backtracking	Adjustment for shade-accounting-tracking systems
Angle Range	Range of single-axis rotation along horizontal axis

Table 1: Inputs to the solar power ANN *reflecting solar site characteristics. Used in conjunction with time-dependent zenith, azimuth, GHI, and temperature features.*

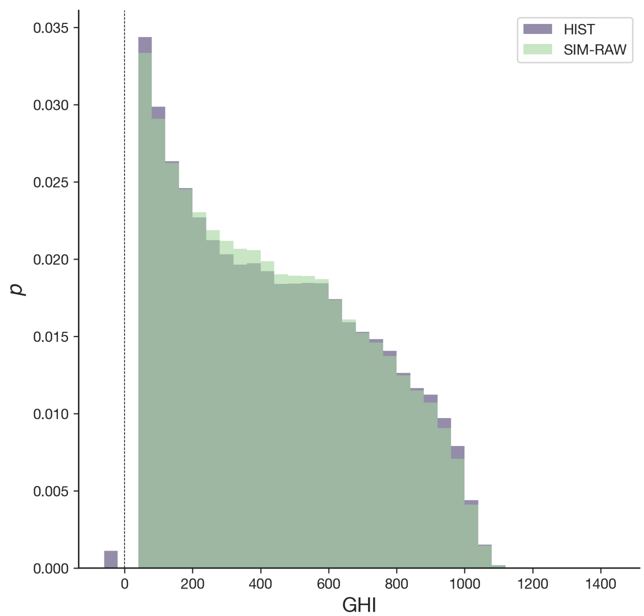

Figure 6: Histograms comparing historical and generated simulation hourly GHI *across all sites. Bins are $40W/m^2$ wide; p is the proportion of data in each bin. As half of the GHI values were 0 (i.e. night-time), the shaded difference in p for the $[0, 40)$ bin is given in a column to the left. Historical and Simulation distributions are very similar.*

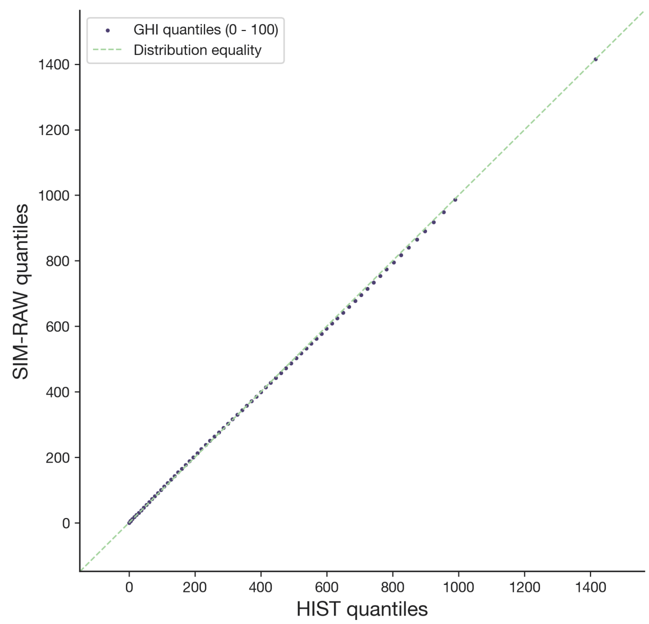

Figure 7: QQ plot of historical and simulation hourly GHI distributions *on all sites. Points are quite close to the line indicating distribution equality.*

3.1 Simulation validation

3.1.1 Hourly GHI distributions

Histogram: Figure 6 shows a histogram of hourly GHI readings across all sites in the HIST and SIM-RAW datasets. The distributions are visually quite close with a slight deviation in SIM-RAW values towards the center of the distribution. A histogram of hourly GHI readings for a sample site can be found in Appendix C.

QQ plot: Figure 7 shows a QQ plot of the HIST and SIM-RAW hourly GHI readings across all sites with a reference line at $y = x$ plotted that corresponds to distribution equality (i.e., the condition where the simulation quantiles match the historical quantiles). The axes of the QQ plot range from 0.5 to 1 as around half of the predicted GHI values in both datasets were identically 0. A QQ plot of hourly GHI readings for a sample site can also be found in Appendix C.

3.1.2 Annual GHI distributions and generation

Mean and median GHI and production numbers across all sites and meteorological years are shown in Table 2.[13] While HIST GHI and generation means were slightly higher than their SIM-RAW counterparts, this pattern was reversed when we consider medians.

[13] For median numbers, we take the median at each site and then take the mean of the medians.

	GHI	AC
HIST	198.53 (198.62)	0.2844 (0.2845)
SIM-RAW	197.97 (198.63)	0.2838 (0.2847)

Table 2: GHI (W/m^2) and production (AC capacity factor) *over all sites. Medians are in parentheses;* HIST *and* SIM-RAW *GHI and Production are close.*

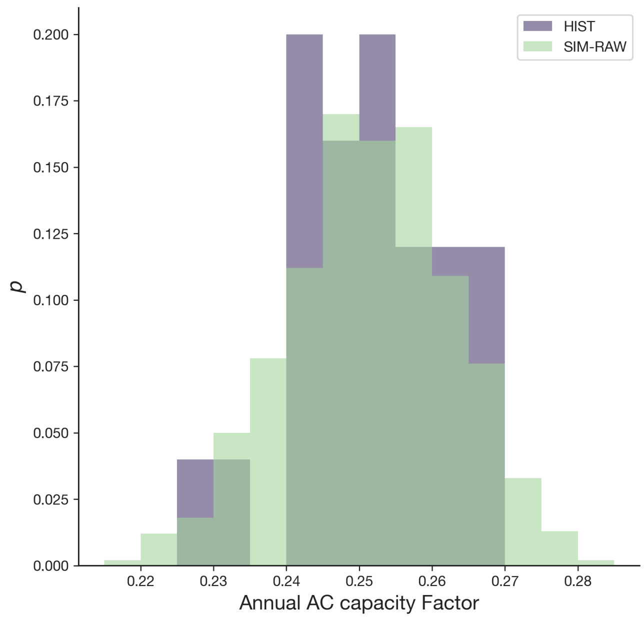

Figure 8: Annual production distributions *at Two Creek Solar (Wisconsin Public Service Corp.).* SIM-RAW, *as it contains 40x more data, is smoother and more complete than the noisy* HIST *distribution. Note that due to limited data,* HIST *lacks samples of the extremes.*

In terms of standard error (Appendix E), we found SIM-RAW GHI means (medians) to be on average 0.69 (0.53) units of standard error from the HIST estimates; generation means (medians) were on average 0.53 (0.56) apart. In other words, the differences between HIST and SIM-RAW were smaller in magnitude than error the in the HIST estimates themselves.

On a site-by-site basis, we also performed t-tests to compare annual GHI and generation numbers between the 25 historical years and 1000 simulation runs. We did not find significant differences in annual GHI (AC capacity factor) means at 99 (100) of the 100 sites ($p > 0.05$).[14]

Figure 8 displays the distributions of one solar site's mean annual AC capacity factors.

[14] Even if the distributions were identical, we would expect 5 of the 100 to have significant differences, so a small number of sites with a significant difference is not surprising.

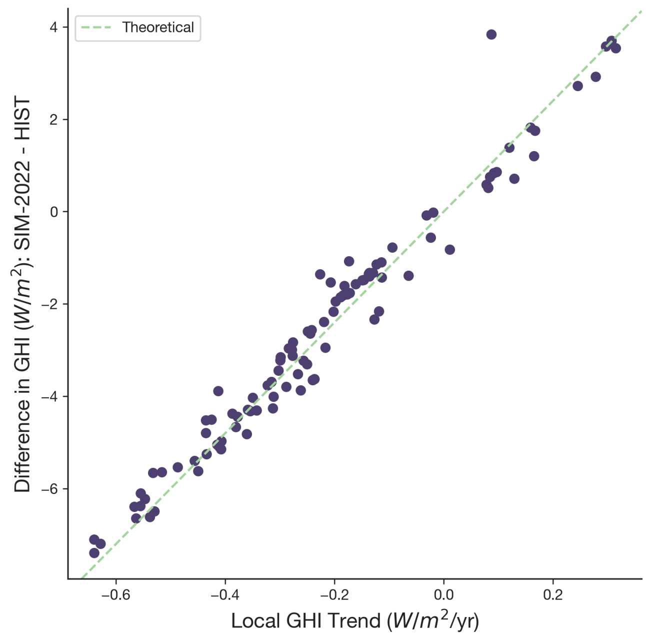

Figure 9: Climate trend adjustment validation *showing detected site GHI trend (x-axis) and differences between mean trend adjusted simulation GHI and historical GHI (y-axis). Local GHI trends are reflected in simulation GHI as expected.*

3.2 Trend extrapolation

Having verified that the stochastic simulations produced realistic weather, we verified that our stochastic *climate* simulations accounted for GHI trends as expected.

Given a site annual GHI trend of γ, we expected mean SIM-2022 GHI to be 12γ higher than mean HIST GHI.[15]. Figure 9, which plots each site's detected GHI trend against differences in mean GHI between SIM-2022 and HIST shows this to be the case.

SIM-2034 was also able to extend GHI trends as expected — Figure 10 plots detected GHI trends against differences in mean GHI between SIM-2034 and SIM-2022.

Figure 11 shows annual historical and simulated mean GHI values for the Miami-Dade Solar Energy Center (FPL) as well as the detected trend on historical values. We note that SIM-2022 is in line with this trend and that the trend was successfully extended out to 2034.

4 Results

We first remark that as irradiance is much more impactful than temperature for PV production at the scale of the climate trends and differences that we see ([15], [16]), we focus on GHI and generation statistics.

[15] Assuming linear trends, SIM-2022 should be on average 12 years of trend from the 1998-2022 historical means.

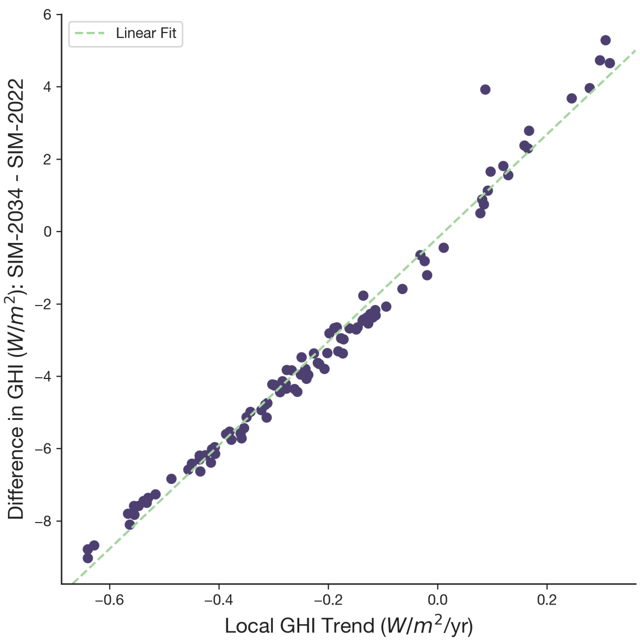

Figure 10: Climate trend extrapolation validation *showing detected site GHI trend (x-axis) against differences in mean GHI between* SIM-2034 *and* SIM-2022 *simulations. Differences correctly reflect 12 years of additional climate trends.*

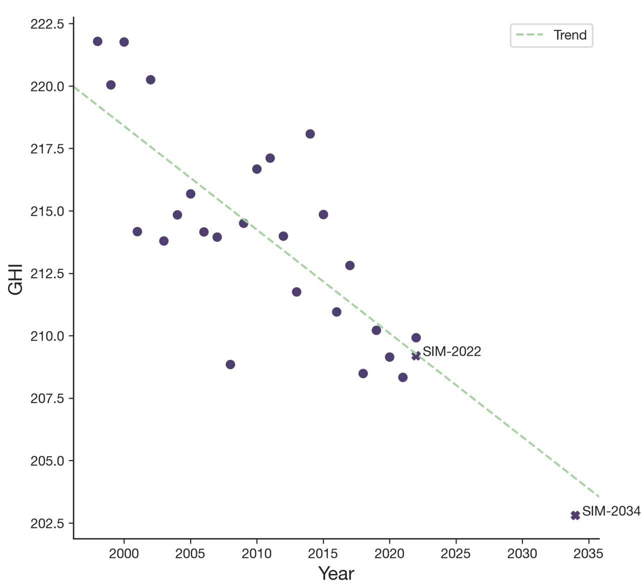

Figure 11: Annual GHI averages *at the Miami-Dade Solar Energy Center. Simulation GHI averages for 2022 and 2034 are in line with the detected negative trend.*

Generation statistics are reported via modeled AC capacity factor. When reporting exceedance values, we follow the industry convention that a PY value is *exceeded* Y% of the time.[16]

We note four major results:

- TMYs are not typical (Section 4.1).
- TMYs GHI & production are biased (Section 4.2).
- Climate change significantly affects solar production (Section 4.3).
- Stochastic simulation reduces uncertainty in production estimates (Section 4.4).

Summary Statistics comparing TMY, HIST, and SIM are given in (Section 4.5).

4.1 TMYs are not typical

In our data, the TMY algorithm did not generate typical years. Rather, *TMY years were idealized years with lower variance than real life.*

Given a solar site and a calendar month m, we calculated the mean GHI reading for each of the 25 examples of m in the historical data[17]. We then converted these into z-scores using the historical mean and standard deviation.[18]

If the process of selecting months for use in a TMY preserved historical variance, the 1200 selected z-scores across all TMY months (100 sites, 12 calendar years) and sites should follow a similar distribution to the 30000 z-scores across all historical months and sites. (100 sites, 12 calendar months, 25 years of data) As Figure 12 shows, this is not the case.

The standard deviation of TMY-selected months (0.43) is about half that of the historical distributions (0.98) — reflecting the creation of years that feature much less month-to-month variation than real life.

Additional evidence of the atypicality of TMYs via mean monthly Finkelstein-Schafer statistics is given in Appendix D.

4.2 TMY GHI & production are biased

Perhaps more importantly for solar production risk assessment, *the TMY algorithm produced meteorological years that were biased towards sunny weather.*

In particular, the TMY algorithm selects months from a group of historical months via "typicality" definitions based on rankings — not raw values — and therefore selects months more similar to median months than to mean months. As the monthly historical GHI z-scores from the previous section are left-skewed (Figure 12)[19],

[16]In other words, a P90 value is *lower* than a P50 value while a P10 value is *higher*.
[17]One per historical year.
[18]Calculated on the aforementioned 25 historical samples.
[19]Fisher-Pearson coefficient of skewness of -0.37

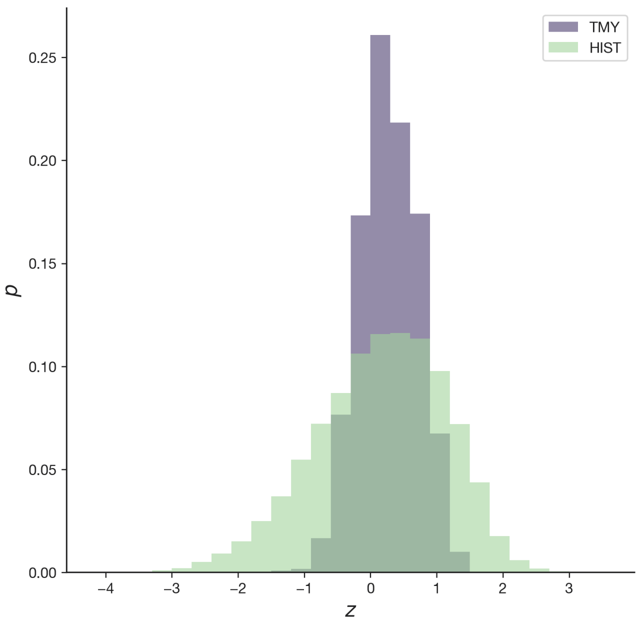

Figure 12: Distribution of monthly GHI z-scores *showing months selected in TMYs to create atypical years with reduced month-to-month variance. Note the left-skew of historical months, which causes the TMY (which selects median-like months) to overpredict GHI.*

	GHI	AC
TMY	200.29	0.2871
HIST	198.53	0.2844

Table 3: Irradiance and production on TMY and historical weather *showing significantly higher ($p <$ 0.001) differences.* TMY *overpredicts* HIST *production by* 0.95%.

this implies that the mean z-score for a TMY-selected month was higher than historical averages — to be precise, 0.13 z-scores higher (a significant ($p < 0.001$) difference).

This positive bias in monthly GHI z-scores was reflected in the irradiance of months chosen by the TMY algorithm — and the resulting power production. Table 3 gives the average GHI readings and AC capacity factors for the two datasets. Paired t-tests of both GHI and generation find the differences to be significant ($p < 0.001$).

Figure 13 shows histograms of the percentage overprediction of TMY vs HIST in annual GHI and AC capacity factor[20]. TMY means (medians) are higher than the historical estimates at 85% (82%) of the solar sites. The TMY generation estimates correspond to an average historical percentile of 62%, i.e. a P38 exceedance value.

In other words, *TMY months presented a significantly sunnier view of history, corresponding to the P38 exceedance level.*

[20]i.e. (TMY − HIST)/HIST ∗ 100.

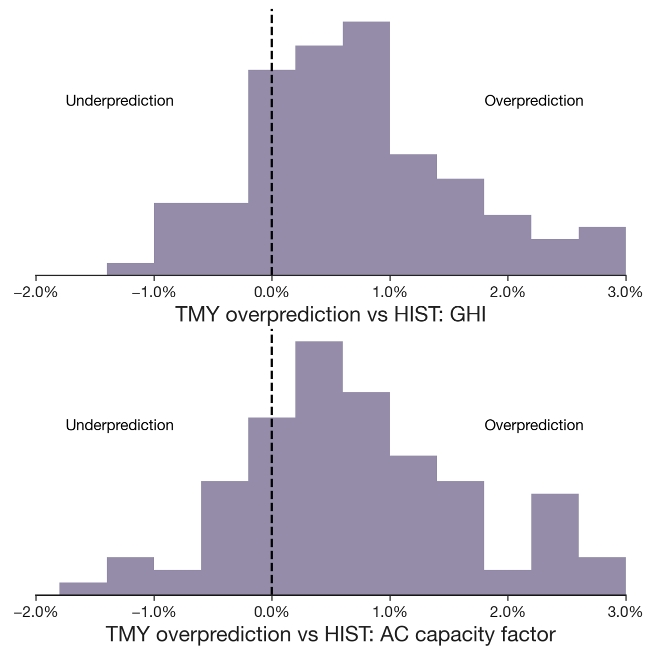

Figure 13: Histograms of percentage differences in GHI and production between TMY and historical averages, *showing* TMY *to overpredict both at the vast majority of the sites.*

4.3 Climate change significantly affects solar production

GHI and power production have a non-linear relationship[21] at an instantaneous and hourly level — underscoring the need for modeling solar production using hourly weather predictions (instead of simple scaling of average annual values). Unsurprisingly, GHI climate trends were consistently reflected in power production predictions.

In addition to having a nonlinear effect on hourly power production, GHI trend adjustments are not applied at night. A 1% change in mean annual GHI, for example, corresponds to a larger change in daylight GHI that is dependent on hour, season, and latitude.

As a result, we found differences in GHI due to climate trends to have an outsized effect on power production predictions. Across all sites, changes in production predictions between HIST and SIM-2022 were 50% larger than changes in GHI predictions. In particular, *the difference in power predictions for 2022 — which are due solely to accounting for climate trends — ranged from -6.16% to 2.77%* of average AC capacity factor.

These differences only rise in magnitude when extending out to 2034, where we find *climate-trend-adjusted differences in power predictions for 2034 from historical averages to range from -13.48% to 4.63%* of average AC capacity factor. The large magnitude and variance of these differences underscores the need to model local

[21]Necessitating models like ours described in Section 2.6.

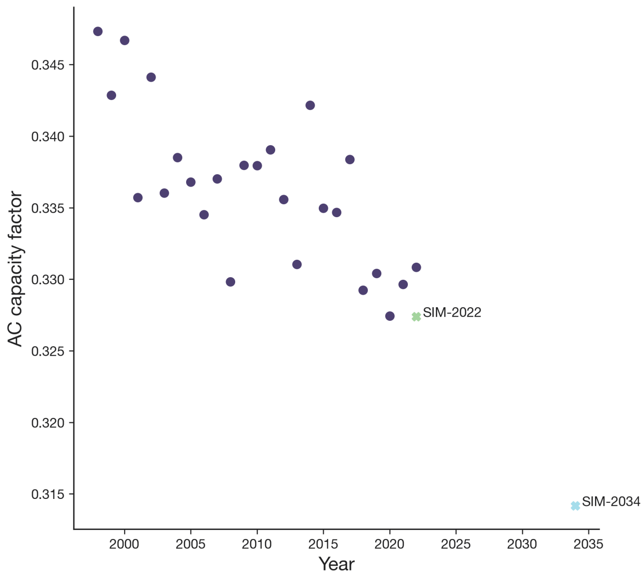

Figure 14: Annual generation *at the Miami-Dade Solar Energy Center. The negative trend in GHI (Figure 11) is accounted for in the* SIM-2022 *simulations and extrapolated to 2034 in the* SIM-2034 *simulations, leading to drops of 2.66% and 6.59% in production from historical means.*

climate trends when modeling solar projects.

Figure 14 shows the power generation analog to Figure 11 at the Miami-Dade Solar Energy Center. We again note that the SIM-2022 data reflects the trend in generation and that this trend is continued in SIM-2034.

4.4 Stochastic simulation reduces uncertainty in production estimates

We explored the degree of uncertainty in each of our datasets, focusing on the more economically pertinent variable of power generation[22].

4.4.1 P50 uncertainty

Table 4 gives the average adjusted standard error (see Appendix E for details) of P50 site annual generation estimates as a percentage of generation predictions. We note that TMYs do not give any estimate of uncertainty, that uncertainty in power generation predictions from historical data is four times higher than uncertainty resulting from simulation, and that average expected uncertainty in P50 estimates from historical data approaches one percent of generation predictions.

4.4.2 Exceedance values

Estimates of exceedance values are more susceptible than mean and median estimates to uncertainty due to small sample sizes — fewer samples lead to fewer rare events, hampering attempts to estimate rare event statistics.

[22]GHI statistics show similar patterns.

	Error
TMY	-
HIST	0.93%
SIM-RAW	0.19%
SIM-2022	0.22%
SIM-2034	0.23%

Table 4: Standard error of median estimates *as a percentage of generation, reflecting the noise inherent in extrapolating from limited historical data and the 4x improved accuracy of Sunairio estimates. Note the inability of the single-year* TMY *to provide error estimates.*

Calculating P90, P95, and P99 estimates on historical data is prone to uncertainty. As an illustration, given 25 years of independent annual generation data, there is an approximately 7.2% chance that *none* of the encountered years is among the true bottom 10% of generation.[23], a 27.7% chance that none is among the true bottom 5%, and a 77.8% chance that none is among the bottom 1%.[24]

We sampled SIM-RAW annual generation data to explore the uncertainty in exceedance values PY as a function of Y and sample size n. From each site's 1000 annual generation numbers, we created 100 samples of n annual generation results with replacement. We then calculated exceedance values on these samples and looked at the standard deviation in the estimates.

Figure 15 shows the results of our bootstrapping tests. As expected, uncertainty in PY increased as we move from the median. All uncertainty was greatly reduced when n increases. In particular, PY uncertainty estimates with $n = 25$ were halved with a larger sample size of $n = 100$. The Sunairio method, simulating 1000 outcomes, would have even lower uncertainty.

4.5 Summary statistics

4.5.1 All sites

Table 5 gives the mean, P50, P90, and P99 values for GHI on each dataset, averaged over all sites.

Empirical HIST estimates are about 1% less than the unreasonably sunny TMYs, SIM-RAW and HIST are quite close, and SIM-2022 and SIM-2034 account for the overall negative trend in GHI as expected.

Paired t-tests of P50 estimates between datasets find significant differences ($p < 0.001$) between TMY and HIST, SIM-RAW and SIM-2022, and SIM-2022 and SIM-2034. Notably, the paired t-tests do not find a significant difference between HIST and SIM-RAW, further validating

[23]$0.9^{25} \approx 0.0719$

[24]These estimates become even higher when we account for the fact that historical samples are autocorrelated.

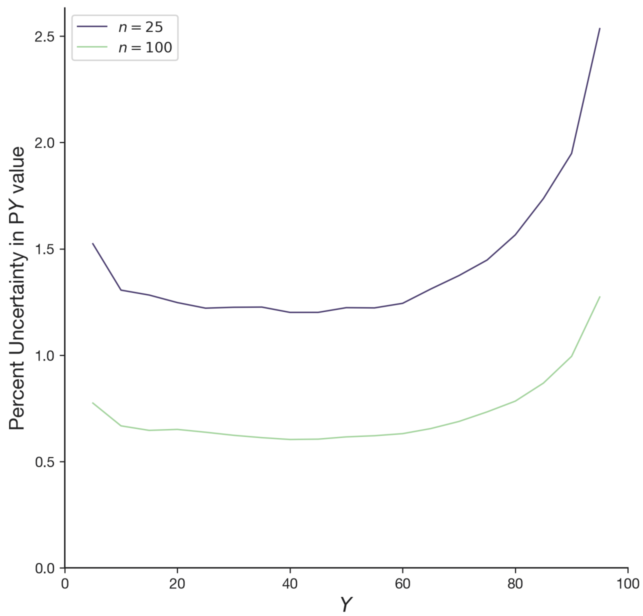

Figure 15: Uncertainty in exceedance values PY *as a function of Y. Uncertainty increases when attempting to account for extreme events and is universally decreased with an increased sample size — highlighting the benefits of simulation over historical estimates.*

that the Sunairio method faithfully reproduces realistic weather.

Turning to generation, Table 6 gives the mean, P50, P90, and P99 values for production on each dataset, averaged over all sites.

We note a 1% drop in AC capacity factor when comparing HIST to TMY, very similar production numbers between HIST and SIM-RAW, and decreasing production when the overall negative trend in GHI is accounted for and extended.

We also see the outsized effect of GHI on production — in particular, the average -3.13% drop in annual site GHI between HIST and SIM-2034 becomes a -4.36% drop in annual site AC capacity factor.

	mean	P50	P90	P99
TMY	200.29	200.29	-	-
HIST	198.53	198.62	191.01	187.61
SIM-RAW	197.97	198.63	186.02	173.99
SIM-2022	195.94	196.59	183.03	169.77
SIM-2034	192.54	193.24	179.53	166.35

Table 5: GHI mean and exceedance values *in W/m^2 over all sites. We see* TMY *overprediction, similarity of* SIM-RAW *and* HIST*, and a overall negative trend in GHI that is accounted for and extended to 2034. Note that the historical P90 and P99 estimates on 25 data points are unreliable.*

	mean	P50	P90	P99
TMY	0.2871	0.2871	-	-
HIST	0.2844	0.2845	0.2728	0.2675
SIM-RAW	0.2838	0.2847	0.2651	0.2470
SIM-2022	0.2795	0.2804	0.2592	0.2392
SIM-2034	0.2724	0.2733	0.2521	0.2327

Table 6: Production mean and exceedance values *in AC capacity factor over all sites. Like in Table 5, we find overprediction by* TMY*, similarity between* HIST *and* SIM-RAW*, and an overall negative trend that is accounted for in* SIM-2022 *and extended in* SIM-2034*. Average percentage loss per site between* TMY *and* SIM-2034 *is 4.98%. Note again that P90 and P99 estimates on* HIST *are unreliable.*

	(+)	(-)
TMY	0.73%	0.97%
HIST	-	-
SIM-RAW	-0.04%	0.07%
SIM-2022	1.65%	-2.19%
SIM-2034	2.35%	-5.43%

Table 7: Average percentage change in P50 production estimate by GHI trend direction *with respect to historical averages, showing continued* TMY *overprediction and similarity between* HIST *and* SIM-RAW *on all sites. Climate trended simulations production estimates on negatively trending GHI sites for the year 2034, for example, are 5.43% less than historical averages.*

4.5.2 Site trends

While 83 of our 100 solar sites had negative GHI trends, the remaining 17 sites became sunnier over the course of the historical data. Table 7 gives the average percentage differences in P50 power generation from historical estimates of each of these sets of solar sites.

Again, TMY overpredicts generation and HIST is quite close to SIM-RAW. Accounting for climate trends results are as expected, with positive trend sites producing more power over time — and negative trend sites producing less power over time. With the exception of HIST and SIM-RAW, paired t-tests find the differences to be significant ($p < 0.001$)

Calculating local climate trends, in other words, can be quite significant.

5 Conclusion

In the original TMY paper [1], the authors wrote the following:

> Weather data are actually a multivariate stochastic process with complex interrelationships among the variables. Fitting multivariate

> stochastic processes with mathematical models is somewhat difficult. Also, even if such models could be derived and a computer simulation performed to generate meteorological data, one would still be faced with the problem of deciding about the typicalness of a set of generated data.
>
> These problems plus time constraints (both chronological and computational) suggested that a more empirical approach for obtaining TMYs might be better.

These words — written before the invention of Linux, MS-DOS, or the Macintosh — reflected the computational and methodological limitations of 1978. Advances in computational power as well as modern techniques for maintaining inter-variable relationships have made complex multivariate stochastic modeling possible.

Executing the TMY authors' vision, the Sunairio method models weather as a multivariate stochastic process that respects a high-dimensional correlation structure. It derives models empirically (reflecting an ongoing paucity in weather data) and can stochastically generate an arbitrary amount of realistic weather data across a fleet of solar sites.

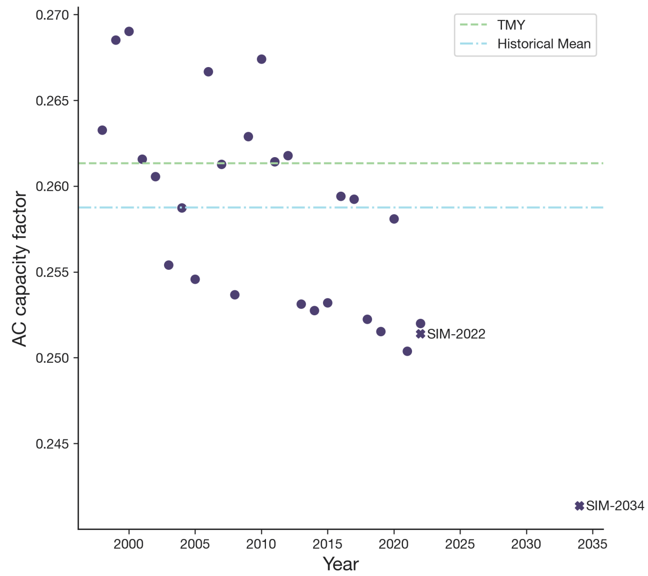

Figure 16: Annual production averages *in AC capacity factor at the FPL Rodeo Solar Energy Center. Note the overprediction of* TMY *with respect to* HIST *and the result of the negative GHI trend on trend-adjusted production estimates for 2022 and 2034 — indicating losses of -2.84% and -6.71% with respect to historical averages respectively.*

5.1 Overview

In this study, we selected a representative sample of 100 solar sites in the continental US. We calculated climate trends and TMYs for each site using 25 years of historical data. We also created weather simulations designed to reflect historical distributions (SIM-RAW) and account for climate trends (SIM-2022 and SIM-2034).

We discovered a negative trend in GHI at 83 of our 100 sites with an overall negative trend of $-0.225W/m^2$/yr.

We found that the TMY algorithm creates years that are not typical and are biased towards higher irradiance. TMY PV generation estimates were higher than historical averages at 85 of the 100 sites with an average of 0.95% production overprediction (Sections 4.1 and 4.2).

Further, we concluded that historical estimates are also unreliable as they fail to account for climate trends (Section 4.3) and are plagued by small sample sizes (Section 4.4). The failure to adjust for climate trends leads to mispredictions ranging from -6.16% to 2.77% of AC capacity factor in current years; small sample sizes lead to expected prediction error from true P50s of 0.93%.

The Sunairio Stochastic Climate Simulation method on the other hand, is able to

- Create weather indistinguishable from historical distributions. (Section 3)
- Generate arbitrary amounts of realistic weather simulation data — thereby enabling analysis of extreme weather events not observed in limited historical data (Section 2.5).
- Properly adjust for local climate trends and extrapolate trend effects into the future, with 2034 production estimates differing from historical averages by -13.48% to 4.63% of AC capacity factor. (Section 4.3).
- Reduce uncertainty in means, medians, and exceedance values estimates. Historical uncertainty in means and medians, for example, was 4x higher than simulation uncertainty (Section 4.4).
- Although general irradiance trends are negative, these trends vary locally in both magnitude and sign — and with magnified effects when considering modeled power generation (Section 4.5).

5.2 Illustrative examples

5.2.1 Negative GHI trend

Consider the FPL Rodeo Solar Energy Center, a 74.5MW solar site in DeSoto county, Florida with a $-0.359W/m^2$/yr GHI trend.

Figure 16 shows modeled solar generation since 1998 as well as the mean climate-adjusted Sunairio generation estimates for 2022 and 2034. Horizontal lines indicate the historical mean generation and TMY estimate.

While the TMY estimate of 0.2613 overestimates the historical mean of 0.2587, the SIM-2022 estimate of 0.2514 and SIM-2034 estimate 0.2414 capture and extend the effects of the local climate trend — and produce gen-

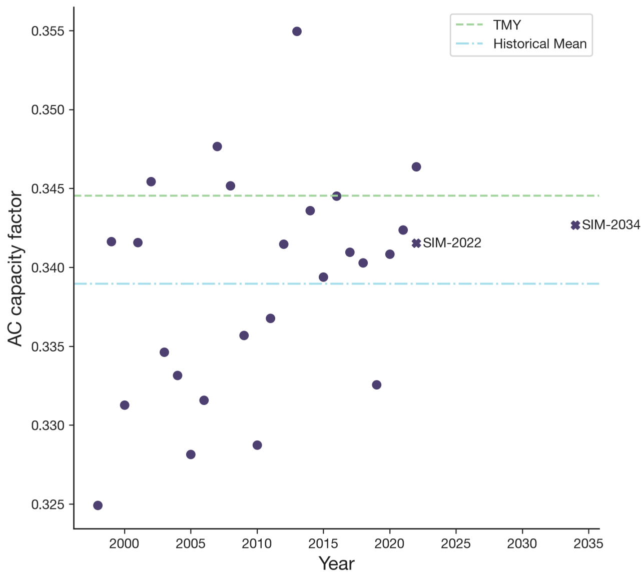

Figure 17: Annual production averages *in AC capacity factor at the PG&E Gates Solar Center. Again, note the overprediction of* TMY *with respect to* HIST *and the influence of the slightly positive GHI trend — leading to modest 2022 and 2034 production gains of 0.76% and 1.10% with respect to historical averages respectively.*

eration predictions that are 3.8% and 7.6% lower than the TMY estimate respectively. Assuming an energy price of $50 per MWh, these overestimations correspond to annual revenue shortfalls of $323,000 and $650,000, respectively.

5.2.2 Positive GHI trend

On a more optimistic note, we now consider the PG&E Gates Solar Center, a 20MW solar site in Kings county, California with a 0.129W/m^2/yr GHI trend. (Figure 17)

Again, the TMY estimate of 0.3445 overestimates the historical mean of 0.3389. The SIM-2022 estimate of 0.3415 and SIM-2034 estimate of 0.3427 reflect a the slight upward trend in irradiation from historical averages — but do not exceed the sunny TMY estimate. Annual revenue shortfalls from TMY estimates are $26,500 and $16,000, respectively.

5.3 Discussion

Solar sites across the US are broadly underperfoming with respect to P50 estimates [17]. While others have investigated underperformance as a result of technical and equipment failures [18], [19], we investigated and discovered additional sources of underperformance due to (i) TMY overprediction and (ii) failure to account for negative trends in irradiance.

The Sunairio method accounts for these biases via stochastic simulations of locally-climate-adjusted weather, which result in demonstrably more accurate and reliable estimates of potential power generation over a long time frame. Combining simulated power predictions with knowledge of regional climate patterns can lead to more diversified solar portfolios and higher overall power generation.

References

[1] I. J. Hall, R. R. Prairie, H. Anderson, and E. C. Boes, "Generation of Typical Meteorological Years for 26 SOLMET Stations," 1978.

[2] T. Cebecauer and M. Suri, "Typical Meteorological Year Data: SolarGIS Approach," in *International Conference on Concentrating Solar Power and Chemical Energy Systems, SolarPACES 2014*, vol. 69, pp. 1958–1969, 2015.

[3] S. Wilcox and W. Marion, "Users Manual for TMY3 Data Sets," Tech. Rep. NREL/TP-581-43156, May 2008.

[4] D. E. Parker, T. P. Legg, and C. K. Folland, "A new daily Central England Temperature series," *International Journal of Climatology*, vol. 12, pp. 317–342, 1992.

[5] M. Sengupta, Y. Xie, A. Lopez, A. Habte, G. Maclaurin, and J. Shelby, "The National Solar Radiation Data Base (NSRDB)," *Renewable and Sustainable Energy Reviews*, vol. 89, pp. 51–60, June 2018.

[6] J. O. Allen, "Improved PV Plant Energy Production Prediction (Phases 1 & 2) The Effect of Short-Term Inverter Saturation on PV Performance Modeling," Tech. Rep. 3002018708, October 2022.

[7] "Annual Electric Generator Report (2021)," *US Energy Information Administration: Independent Statistics and Analysis*, September 2022.

[8] "NSRDB: TMY." https://nsrdb.nrel.gov/data-sets/tmy. Accessed: 2023-07-10.

[9] A. Lauer, L. Bock, B. Hassler, M. Schröder, and M. Stengel, "Cloud Climatologies from Global Climate Models—A Comparison of CMIP5 and CMIP6 Models with Satellite Data," *Journal of Climate*, vol. 36, January 2023.

[10] S. Bony, B. Stevens, D. M. W. Frierson, C. Jakob, M. Kageyama, R. Pincus, T. G. Shepherd, S. C. Sherwood, A. P. Siebesma, A. H. Sobel, M. Watanabe, and M. J. Webb, "Clouds, circulation, and climate sensitivity," *Nature Geoscience*, vol. 8, pp. 261–268, March 2015.

[11] "Annual 2022 Global Climate Report," *NOAA: National Centers for Environmental Information*, January 2023.

[12] K. Hayhoe, D. Wuebbles, D. Easterling, D. Fahey, S. Doherty, J. Kossin, W. Sweet, R. Vose, and M. Wehner, "Our Changing Climate," vol. II, p. 72–144, 2018. In Impacts, Risks, and Adaptation in the United States: Fourth National Climate Assessment.

[13] A. P. Dobos, "PVWatts Version 5 Manual," Tech. Rep. NREL/TP-6A20-62641, September 2014.

[14] W. F. Holmgren, C. W. Hansen, and M. A. Mikofski, "pvlib python: a Python Package for Modeling Solar Energy Systems," *Journal of Open Source Software*, vol. 3, p. 884, September 2018.

[15] J. Adeeb, A. Farhan, and A. Al-Salaymeh, "Temperature Effect on Performance of Different Solar Cell Technologies," *Journal of Ecological Engineering*, vol. 20, no. 5, 2019.

[16] C. Xiao, X. Yu, D. Yang, and D. Que, "Impact of solar irradiance intensity and temperature on the performance of compensated crystalline silicon solar cells," *Solar Energy Materials and Solar Cells*, vol. 128, pp. 427–434, 2014.

[17] kWh Analytics, "2022 Solar Generation Index," 2022.

[18] kWh Analytics, "Solar Risk Assessment: 2023," June 2023.

[19] R. Maps, "Global Solar Report," February 2023.

[20] J. Finkelstein and R. Schafer, "Improved Goodness-of-Fit Tests," *Biometrika*, vol. 58, pp. 641–645, 1971.

[21] N. M. Sawaqed, Y. Zurigat, and H. Al-Hinai, "A step-by-step application of Sandia method in developing typical meteorological years for different locations in Oman," *International Journal of Energy Research*, vol. 29, pp. 723–737, June 2005.

[22] A. Dobos, M. Kasberg, and P. Gilman, "P50/P90 Analysis for Solar Energy Systems Using the System Advisor Model," May 2012.

[23] E. Mackay and P. Jonathan, "Sampling Properties and Empirical Estimates of Extreme Events," *Ocean Engineering*, vol. 239, 2021.

[24] J. R. Bence, "Analysis of Short Time Series: Correcting for Autocorrelation," *Ecology*, vol. 76, no. 2, pp. 628–639, 1995.

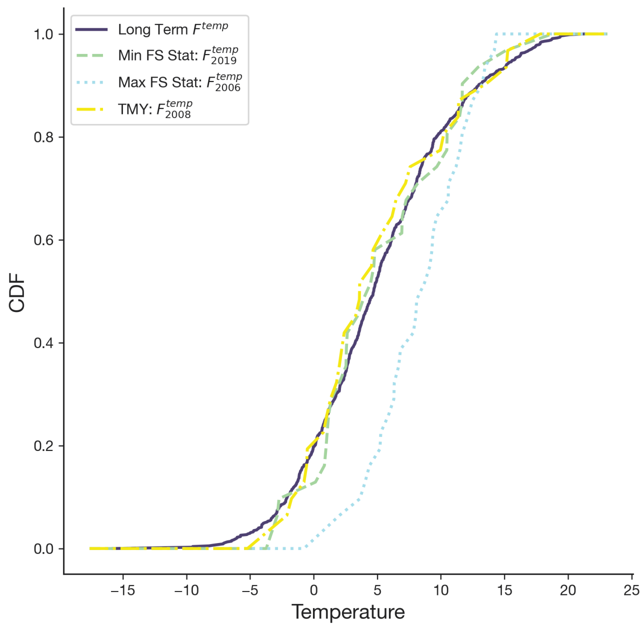

Figure 18: Selected CDFs for January temperatures *at a sample site. 2006 has the largest FS statistic, 2019 has the smallest FS statistic, and 2008 was chosen in the eventual TMY.*

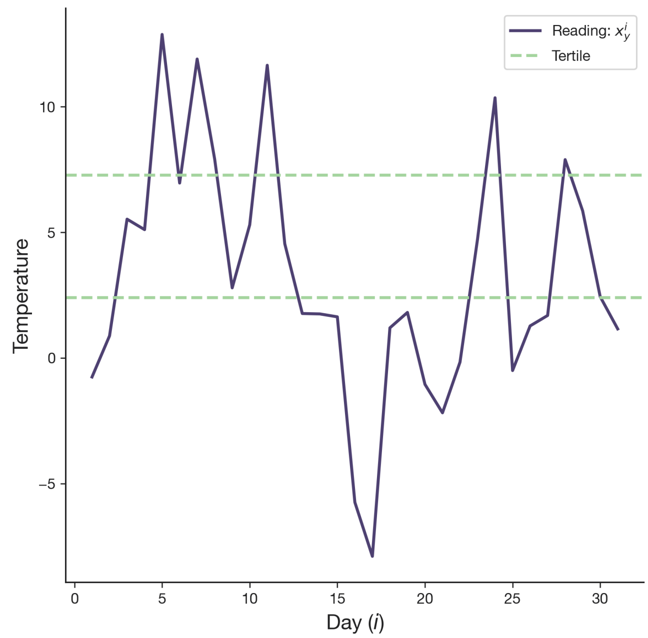

Figure 19: Persistence cutoffs for a candidate month *with 4 streaks in the first tertile and 5 streaks in the third tertile.*

Appendix A TMY3 details

In the following discussion of our re-implementation of TMY3 [3], m is a calendar month with d_m days. The TMY algorithm uses daily-averaged weather readings; for each weather variable x and candidate calendar month from year y we have d_m readings. We define x_y^i as the reading of x on day i in year y

A.1 Finkelstein-Schafer statistics

Given a weather variable x, we defined F_y^x as the Cumulative Distribution Function (CDF) of the d_m sample readings from year y and F^x as the CDF of all $25d_m$ samples from all years.

We defined the Finkelstein-Schafer statistic [20] as

$$FS(y:m,x) = \frac{1}{d_m}\sum_{i=1}^{d_m} |F^x(x_y^i) - F_y^x(x_y^i)|$$

which measures the average distance between the long-term CDF and the CDF for a particular candidate month. Figure 18 displays selected January temperature CDFs for one of the sites.

Each of the 25 candidate months was assigned a score with the weighted sum of these statistics across several weather variables

$$\sum_{x\in\mathcal{X}} w_x FS(y:m,x)$$

where x ranged across temperature, humidity, wind speed, and irradiance with weights w_x of 0.2, 0.2, 0.1, and 0.5 respectively. Candidate months that were not among the five highest-scoring months were discarded.

A.2 Persistence criteria

We calculated tertile boundary values for temperature and irradiance over all $25d_m$ readings. For the 5 remaining candidate months, we then detected streaks of consecutive readings (Figure 19). We considered streaks in the first or third temperature tertiles and streaks in the first irradiance tertile.

We eliminated candidate months that had the most streaks, had the longest streak, or had no streaks.

A.3 Means and medians

Finally, we ranked the remaining candidates by their closeness to the long-term means and medians.

Following [21] with some minor modifications, we calculated the long-term mean μ_x, median $\bar{x}$, and standard deviation σ_x on all $25d_m$ daily readings. Then for a candidate month from year y, we calculated the scaled differences between that month's mean μ_x^y and median $\bar{x}^y$ from the long term values:

$$\frac{1}{\sigma_x}|\mu_x - \mu_x^y| \qquad \frac{1}{\sigma_x}|\bar{x} - \bar{x}^y|$$

The candidate month from year y is then assigned a score equal to the maximum of resulting 4 scaled differences.

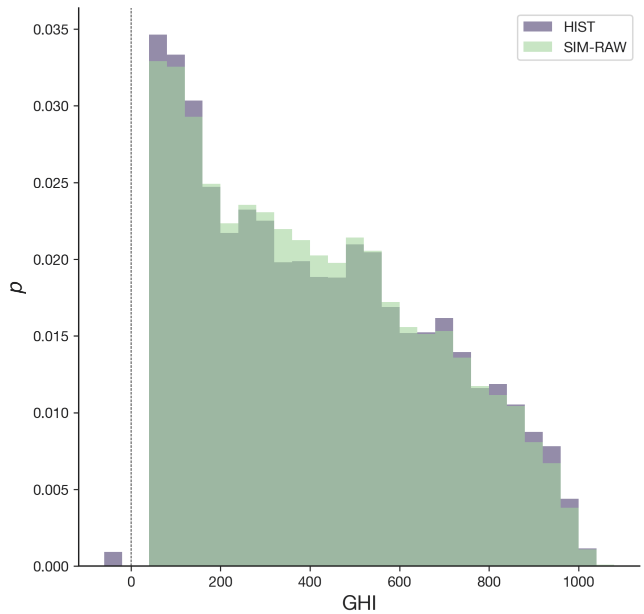

Figure 20: Hourly GHI histogram *at a sample site. Bins are 40W/m^2 wide; p is the proportion of data in each bin. As half of the GHI values were 0 (i.e. night-time), the shaded difference in p for the* $[0, 40)$ *bin is given in a column to the left. Historical and Simulation distributions are very similar.*

We selected the candidate month with the smallest score to represent m in the TMY.

Appendix B ANN validation

Tables 8 and 9 give state capital validation numbers for the solar model using single-axis and fixed-tilt tracking configurations respectively.

Appendix C Site distributions

For a sample solar site, Figure 20 and Figure 21 show a histogram and a QQ plot of hourly GHI for HIST and SIM-RAW data. We see similar patterns to Figure 6 and Figure 7 — except with less data and thus more noise.

Appendix D Mean FS statistics

As discussed in Section A.1, Finkelstein-Schafer statistics $FS(y : m, x)$ measure how "typical" a particular month is when compared to the long-term average for that calendar month.

For a given weather variable x and a meteorological year y, we calculated the mean Finkelstein-Schafer statistic of the constituent months — in other words, the average "typicality" of the months.

	PVWatts	ANN	% Difference
Alabama	474,183	472,803	0.291
Arizona	587,821	586,843	0.166
Arkansas	456,425	455,910	0.113
California	532,209	528,125	0.767
Colorado	497,571	494,314	0.655
Connecticut	401,063	399,521	0.384
Delaware	421,281	422,446	0.277
Florida	475,489	474,613	0.184
Georgia	459,767	458,818	0.206
Idaho	467,087	464,127	0.634
Illinois	422,488	421,267	0.289
Indiana	408,610	408,898	0.070
Iowa	416,416	415,665	0.180
Kansas	442,309	441,516	0.179
Kentucky	416,722	416,859	0.033
Louisiana	472,773	473,348	0.122
Maine	398,138	398,109	0.007
Maryland	424,475	424,930	0.107
Massachusetts	408,832	406,648	0.534
Michigan	389,726	389,655	0.018
Minnesota	400,448	399,999	0.112
Mississippi	465,113	463,899	0.261
Missouri	429,237	429,848	0.142
Montana	415,282	412,842	0.588
Nebraska	445,284	442,353	0.658
Nevada	551,993	547,236	0.862
New Hampshire	396,555	395,098	0.367
New Jersey	409,334	409,253	0.020
New Mexico	562,125	554,936	1.279
North Carolina	450,837	450,446	0.087
North Dakota	418,739	417,789	0.227
New York	390,804	390,358	0.114
Ohio	396,075	395,658	0.105
Oklahoma	486,551	483,433	0.641
Oregon	387,978	386,152	0.471
Pennsylvania	407,019	406,130	0.218
Rhode Island	410,230	408,576	0.403
South Carolina	464,989	465,128	0.030
South Dakota	431,978	432,800	0.190
Tennessee	424,522	423,895	0.148
Texas	480,074	480,521	0.093
Utah	479,750	477,043	0.564
Vermont	372,626	372,554	0.019
Virginia	430,515	431,760	0.289
Washington	342,529	342,465	0.019
West Virginia	400,870	400,640	0.057
Wisconsin	398,653	396,899	0.440
Wyoming	470,745	467,879	0.609

Table 8: Annual DC MWh *on single-axis tracking solar sites at 48 state capitals — for solar model validation*

	PVWatts	ANN	% Difference
Alabama	403,057	400,983	0.515
Arizona	487,189	485,426	0.362
Arkansas	388,616	387,379	0.318
California	438,919	437,483	0.327
Colorado	422,382	420,605	0.421
Connecticut	347,174	346,023	0.332
Delaware	367,377	365,983	0.379
Florida	400,587	398,536	0.512
Georgia	388,328	386,279	0.528
Idaho	387,670	386,291	0.356
Illinois	361,119	359,489	0.451
Indiana	350,868	350,257	0.174
Iowa	359,205	358,505	0.195
Kansas	383,936	382,500	0.374
Kentucky	355,811	354,731	0.304
Louisiana	398,340	397,407	0.234
Maine	345,022	345,058	0.010
Maryland	368,214	367,360	0.232
Massachusetts	353,494	352,189	0.369
Michigan	333,242	332,883	0.108
Minnesota	346,474	346,036	0.126
Mississippi	393,701	392,179	0.387
Missouri	371,620	371,005	0.165
Montana	352,526	352,484	0.012
Nebraska	383,731	381,954	0.463
Nevada	454,843	452,627	0.487
New Hampshire	343,048	342,204	0.246
New Jersey	356,626	355,686	0.264
New Mexico	463,195	459,207	0.861
North Carolina	387,535	386,341	0.308
North Dakota	358,752	358,551	0.056
New York	337,406	336,855	0.163
Ohio	340,207	339,395	0.239
Oklahoma	410,222	407,891	0.568
Oregon	325,906	325,737	0.052
Pennsylvania	351,286	350,287	0.284
Rhode Island	355,134	353,540	0.449
South Carolina	395,800	394,454	0.340
South Dakota	373,831	374,238	0.109
Tennessee	362,090	360,819	0.351
Texas	406,283	404,528	0.432
Utah	401,929	400,613	0.327
Vermont	323,764	323,289	0.147
Virginia	371,423	370,665	0.204
Washington	292,743	293,167	0.145
West Virginia	344,023	343,076	0.275
Wisconsin	343,948	342,609	0.389
Wyoming	400,842	398,908	0.482

Table 9: Annual DC MWh *on fixed-tilt solar sites at 48 state capitals — for solar model validation*

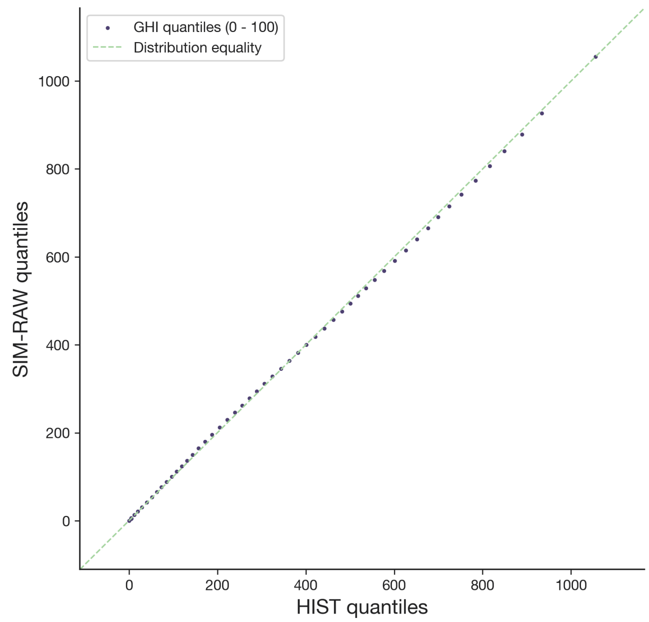

Figure 21: QQ plot of historical and simulation hourly GHI distributions *at a sample site. Points are quite close to the line indicating distribution equality.*

	mean	std
TMY	0.046	0.005
HIST	0.076	0.016

Table 10: Distribution statistics of yearly averages of monthly Finkelstein-Schafer statistics *indicating a reduced mean and standard deviation of* TMY *scores.* TMY *years, in other words, are atypical — in that their constituent months are too typical.*

$$FS(y:x) = \frac{1}{12}\sum_{m} FS(y:m,x)$$

We compared the distributions of $FS(y:GHI)$ between the TMYs and the historical calendar years over all sites. Figure 22 displays distribution box plots; Table 10 gives the means and standard deviations of the distributions.

A simple t-test showed the markedly lower average Finkelstein-Schafer statistics in TMYs to be significantly different than raw historical years ($p < 0.001$). The months in the TMYs, in other words, were not typical.

Appendix E Distribution estimates

E.1 Exceedance values

In addition to considering means and medians, it is common in the solar industry to consider "exceedance" values and probabilities. Given a random variable X and

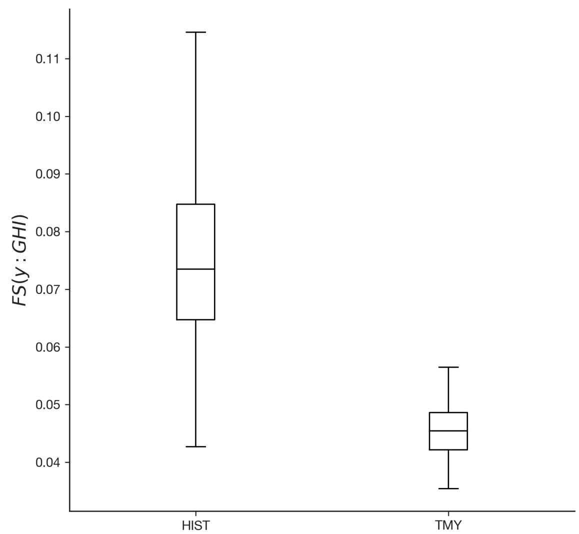

Figure 22: Boxplots of yearly averages of monthly Finkelstein-Schafer statistics *showing* TMY *years to contain months that have lower FS-statistics on average than historical years*

a probability threshold $Y \in [0, 100]$, a PY exceedance value of X is loosely defined as a value x which is exceeded Y percent of the time. A "P90" value, for example, is expected to be exceeded 90% of the time.

$$\mathbb{P}(X \geq x) = Y/100$$

As the true distribution of X is generally not known, one resorts to estimation methods to calculate exceedance values in practice — e.g. via fitting normal distributions or interpolating empirical CDFs. [22]

We found both of these methods to give similar results. Given the skewness and non-normality of the distributions encountered, we report exceedance values via empirical CDF interpolation.[25]

We note that the P50 value of a set of values corresponds to its median.

E.2 Uncertainty

Given a sample of n Independent and Identically Distributed (IID) values from a random variable X, one can estimate the true mean via the sample mean. Given many samples, one can calculate many estimates of the true mean — the standard deviation of these estimates is the "standard error of the mean" and is given by

$$\frac{\sigma}{\sqrt{n}}$$

where σ is the standard deviation of X. As σ is not known in practice, it is often estimated with the sample standard deviation.

The "standard error of the median" is a bit larger. Assuming normality, it is given by

$$\sqrt{\frac{\pi}{2}} \cdot \frac{\sigma}{\sqrt{n}}$$

Uncertainty in quantile estimates (and thus exceedance values) is dependent on the estimation method used.

In our study, simulations runs were by design independent of each other. Annual historical values, however, are correlated year-to-year — and thus not IID. Thus, we further adjusted our historical uncertainty estimates by a correction factor of

$$\sqrt{\frac{1+\rho}{1-\rho}}$$

where ρ is the Prais-Winsten autocorrelation coefficient [24].

Analytic derivation of the standard error of exceedance values is more computationally demanding, depends on the quantile estimation method used, and is dependent on assumptions on the underlying distribution. As a result, we also estimated uncertainty in exceedance values empirically via bootstrapping from simulation results.

[25] Following [23], we estimated empirical CDFs as in expectation, where the k-th ranked value among n values is the expected $\frac{k}{n+1}$ percentile.

Appendix F All solar sites

Table 11: Selected solar sites for the study *with* TMY *and* HIST *production as well as* SIM-YYYY *production percentage differences from* HIST

					HIST			SIM-2022			SIM-2034		
Solar Site	State	DC/AC	MW	TMY	P10	P50	P90	P10	P50	P90	P10	P50	P90
Agua Caliente Solar Project	AZ	1.28	91	0.3480	0.3533	0.3454	0.3390	0.8%	-0.9%	-5.2%	-1.1%	-3.3%	-7.4%
Albemarle Beach Solar	NC	1.88	80	0.3382	0.3441	0.3317	0.3191	1.8%	0.7%	-1.8%	0.7%	-0.6%	-2.9%
Alpine Solar	CA	1.31	66	0.3502	0.3552	0.3501	0.3405	1.8%	-0.6%	-3.0%	1.1%	-1.2%	-4.0%
American Falls Solar	ID	1.30	20	0.2727	0.2832	0.2736	0.2620	3.3%	1.4%	-0.3%	3.9%	2.2%	0.2%
Apple Campus 2 PV	CA	1.10	14	0.2694	0.2750	0.2678	0.2563	6.5%	2.6%	-2.7%	8.2%	4.2%	-1.1%
Assembly Solar II LLC	MI	1.47	110	0.2603	0.2722	0.2557	0.2472	-3.2%	-4.0%	-8.9%	-9.4%	-10.6%	-15.3%
Augusta PV - BD Solar Augusta LLC	ME	1.21	7	0.2161	0.2284	0.2188	0.2099	0.9%	0.2%	-1.6%	0.4%	-0.4%	-2.1%
Aulander Holloman Solar, LLC	NC	1.56	80	0.3003	0.3151	0.3023	0.2911	1.3%	-0.1%	-2.9%	0.0%	-1.6%	-4.7%
Avalon Solar II	AZ	1.34	16	0.3517	0.3547	0.3480	0.3410	2.7%	-0.5%	-5.7%	1.5%	-2.4%	-7.3%
BC Solar	OR	1.31	8	0.2861	0.2983	0.2847	0.2700	5.1%	3.0%	-0.7%	6.7%	4.6%	1.5%
Battle Mountain Solar Project	NV	1.22	101	0.2808	0.2925	0.2788	0.2700	2.8%	1.9%	-2.4%	3.4%	2.3%	-1.6%
Beaver Run	NJ	1.35	7	0.2516	0.2601	0.2492	0.2313	-0.6%	-2.9%	-3.5%	-3.3%	-6.4%	-7.8%
Bluebell Solar II	TX	1.30	115	0.3206	0.3344	0.3223	0.3076	1.5%	-1.9%	-6.1%	-0.9%	-4.2%	-8.4%
Blythe Solar IV, LLC	CA	1.12	69	0.3144	0.3157	0.3092	0.3035	1.6%	-0.7%	-4.9%	0.1%	-2.5%	-6.7%
Buckleberry Solar	NC	1.44	52	0.2932	0.3050	0.2925	0.2790	0.9%	-1.0%	-3.7%	-1.1%	-2.8%	-5.6%
Clark Road Solar 1, LLC	MA	1.42	5	0.2621	0.2709	0.2570	0.2458	-0.2%	-1.3%	-3.7%	-2.1%	-3.4%	-6.2%
Clifton Park Solar 1, LLC	NY	1.50	5	0.2653	0.2763	0.2640	0.2486	-0.1%	-2.4%	-3.7%	-2.3%	-4.5%	-6.6%
Comanche Solar	CO	1.25	120	0.2984	0.3106	0.2987	0.2910	0.6%	-1.9%	-6.3%	-2.4%	-4.8%	-9.8%
Coniglio Solar	TX	1.36	124	0.3042	0.3110	0.2957	0.2799	0.2%	-3.9%	-9.1%	-4.8%	-9.0%	-14.5%
Cotton Creek Solar Energy Center	FL	1.41	74	0.3031	0.3150	0.3014	0.2862	-0.3%	-3.7%	-7.8%	-4.4%	-7.8%	-12.7%
Dane County Airport Solar	WI	1.06	11	0.2028	0.2128	0.1995	0.1889	-3.2%	-4.9%	-9.0%	-9.3%	-11.5%	-15.3%
Decatur Parkway Solar Project, LLC	GA	1.38	80	0.3020	0.3187	0.3015	0.2882	0.3%	-2.3%	-7.2%	-3.6%	-5.8%	-11.0%
Deming Solar Energy Center	NM	1.24	5	0.3342	0.3409	0.3320	0.3216	1.8%	-0.9%	-5.3%	-0.1%	-3.4%	-7.7%
Erwin Farm	NC	1.02	5	0.2166	0.2253	0.2132	0.2058	0.3%	-0.4%	-4.2%	-1.4%	-2.1%	-6.0%
Escalante Solar III, LLC	UT	1.32	80	0.3128	0.3201	0.3093	0.3014	3.5%	1.5%	-2.8%	3.9%	1.6%	-2.6%
Flatwood Farm	NC	1.30	5	0.2716	0.2835	0.2697	0.2572	0.7%	-0.6%	-3.0%	-1.0%	-2.1%	-5.2%
Fort Detrick Solar PV	MD	1.18	16	0.2283	0.2405	0.2315	0.2165	-0.9%	-4.9%	-6.5%	-5.3%	-9.8%	-12.3%
GMP Solar/Storage-Milton Hybrid	VT	1.40	5	0.2412	0.2512	0.2373	0.2265	-0.2%	-0.7%	-3.4%	-1.7%	-2.4%	-4.9%
Gates Solar Station	CA	1.39	20	0.3445	0.3469	0.3408	0.3285	3.8%	0.7%	-2.6%	4.2%	1.0%	-1.9%
Grand View Solar Two	ID	1.35	60	0.2889	0.2954	0.2848	0.2720	3.8%	1.6%	-1.6%	4.8%	2.2%	-0.8%
Great Valley Solar Portfolio Holdings, LLC	CA	1.41	60	0.3402	0.3487	0.3393	0.3268	2.8%	1.1%	-1.8%	3.4%	1.6%	-0.9%
HL Solar	CA	1.22	8	0.2906	0.2981	0.2873	0.2739	4.6%	3.0%	-0.1%	6.2%	4.2%	1.9%
Harmony Solar	FL	1.55	74	0.3344	0.3441	0.3336	0.3232	1.3%	-2.7%	-7.5%	-2.6%	-6.5%	-11.3%
Harry Allen Solar Energy LLC	NV	1.24	100	0.3239	0.3325	0.3239	0.3165	2.6%	0.7%	-3.6%	2.3%	-0.0%	-4.4%
Held Solar Project	MN	1.50	5	0.2745	0.2786	0.2706	0.2584	0.1%	-2.6%	-4.6%	-3.2%	-6.1%	-7.9%

Table 11: Selected solar sites for the study *with* TMY *and* HIST *production as well as* SIM-YYYY *production percentage differences from* HIST

Solar Site	State	DC/AC	MW	TMY	HIST P10	HIST P50	HIST P90	SIM-2022 P10	SIM-2022 P50	SIM-2022 P90	SIM-2034 P10	SIM-2034 P50	SIM-2034 P90
Hillcrest Solar	OH	1.32	200	0.2569	0.2627	0.2511	0.2379	-2.1%	-5.3%	-8.4%	-7.7%	-11.3%	-14.8%
Hooper Solar	CO	1.12	52	0.2805	0.2861	0.2758	0.2667	0.8%	-0.2%	-2.4%	0.7%	-0.5%	-3.1%
Imeson Solar	FL	1.80	5	0.3431	0.3611	0.3438	0.3333	1.1%	-1.1%	-6.8%	-2.4%	-4.7%	-10.3%
Innovative Solar 37 LLC	NC	1.10	100	0.2354	0.2449	0.2313	0.2219	-0.4%	-1.4%	-4.9%	-3.4%	-4.2%	-8.0%
Innovative Solar 43, LLC	NC	1.00	51	0.2118	0.2195	0.2074	0.2010	0.2%	-0.8%	-5.2%	-2.5%	-3.4%	-8.2%
Intel Folsom Phase 3	CA	1.25	5	0.3033	0.3070	0.2986	0.2861	5.0%	2.1%	-2.0%	6.5%	3.2%	-0.8%
Juno Solar Project	TX	1.37	141	0.3390	0.3451	0.3343	0.3210	2.4%	-1.1%	-5.5%	0.7%	-3.0%	-7.7%
Lily Solar Hybrid	TX	1.23	147	0.2846	0.2900	0.2752	0.2607	-0.5%	-3.8%	-8.4%	-5.0%	-8.2%	-13.0%
Macho Springs	NM	1.17	55	0.3205	0.3234	0.3165	0.3054	2.3%	-1.8%	-6.5%	-0.3%	-4.6%	-9.6%
Marlin Solar	TX	1.36	5	0.3035	0.3161	0.3027	0.2854	0.6%	-3.3%	-7.3%	-3.5%	-7.1%	-11.4%
Marshall Solar Energy Project	MN	1.50	62	0.2820	0.2846	0.2750	0.2616	0.2%	-2.0%	-3.9%	-3.1%	-5.7%	-7.5%
Meadowbrook Solar Farm	NC	1.36	5	0.2902	0.2958	0.2819	0.2691	0.2%	-1.4%	-5.1%	-2.8%	-4.6%	-8.2%
Mesquite Solar 1	AZ	1.41	10	0.3680	0.3725	0.3669	0.3594	1.4%	-1.0%	-5.2%	-0.3%	-3.3%	-7.3%
Miami Dade Solar Energy Center	FL	1.52	74	0.3445	0.3452	0.3360	0.3295	2.1%	-2.3%	-8.1%	-1.9%	-6.4%	-11.9%
Midway Solar - TX	TX	1.30	182	0.3312	0.3414	0.3278	0.3154	0.8%	-1.7%	-6.7%	-2.0%	-4.7%	-9.9%
Millican Solar Energy LLC	OR	1.10	70	0.2293	0.2365	0.2282	0.2198	3.7%	1.4%	-1.4%	5.0%	2.7%	-0.5%
Millington Solar Farm	TN	1.32	53	0.2752	0.2874	0.2744	0.2570	-2.3%	-5.2%	-8.1%	-8.7%	-11.8%	-14.4%
Misae Solar	TX	1.36	240	0.3312	0.3336	0.3220	0.3109	1.7%	-1.4%	-6.2%	-0.6%	-3.6%	-8.3%
Moffett Solar Project	SC	1.31	71	0.2826	0.2959	0.2806	0.2670	0.1%	-2.5%	-6.5%	-3.3%	-5.6%	-10.3%
North Star Solar Project	MN	1.38	100	0.2605	0.2632	0.2525	0.2437	-1.2%	-3.3%	-7.4%	-6.2%	-8.9%	-12.7%
Nutmeg Solar	CT	1.61	20	0.2808	0.2928	0.2800	0.2658	0.1%	-1.6%	-3.8%	-2.3%	-4.3%	-6.9%
OCI Alamo 3 LLC	TX	1.22	6	0.2794	0.2921	0.2807	0.2596	0.7%	-3.8%	-6.5%	-3.5%	-7.8%	-11.2%
Old Wire Farm	NC	1.42	5	0.2980	0.3085	0.2908	0.2813	0.4%	0.2%	-3.8%	-1.4%	-1.9%	-5.8%
Oxy Renewable Energy - Goldsmith	TX	1.16	17	0.3041	0.3131	0.3037	0.2908	1.8%	-2.1%	-6.9%	-0.8%	-4.9%	-9.7%
Payne Creek Solar	FL	1.21	70	0.2777	0.2926	0.2813	0.2727	0.1%	-3.4%	-9.7%	-3.9%	-8.0%	-14.4%
Pleinmont Solar 2	VA	1.23	240	0.2514	0.2533	0.2456	0.2308	0.2%	-2.4%	-2.7%	-2.2%	-4.8%	-5.7%
Poseidon Solar, LLC	AZ	1.19	20	0.3210	0.3264	0.3198	0.3103	1.6%	-1.1%	-4.9%	-0.3%	-3.3%	-7.0%
RE Columbia Two, LLC	CA	1.29	15	0.3484	0.3558	0.3501	0.3410	2.0%	-0.5%	-3.6%	1.0%	-1.6%	-5.0%
RP-Orlando, LLC	FL	1.16	5	0.2578	0.2713	0.2586	0.2488	0.2%	-2.9%	-8.0%	-3.9%	-6.9%	-12.0%
Red Horse 2	AZ	1.49	51	0.3681	0.3758	0.3673	0.3612	2.4%	-0.9%	-6.3%	0.4%	-3.0%	-8.3%
Ridgeland Solar Project	SC	1.22	10	0.2662	0.2785	0.2638	0.2516	0.5%	-2.5%	-7.2%	-3.4%	-5.8%	-11.1%
Rock Solid	NJ	1.24	8	0.2425	0.2488	0.2382	0.2198	-1.1%	-4.8%	-5.6%	-5.2%	-9.3%	-11.0%
Rodeo Solar Center	FL	1.11	74	0.2613	0.2678	0.2592	0.2518	1.3%	-2.6%	-8.5%	-2.4%	-6.7%	-12.7%
Rowe (CSG)	NY	1.44	5	0.2443	0.2571	0.2456	0.2318	-0.4%	-3.4%	-5.7%	-4.0%	-7.0%	-10.3%
SID Solar I, LLC	NC	1.28	5	0.2740	0.2832	0.2724	0.2574	-0.0%	-2.5%	-4.3%	-3.0%	-5.2%	-7.3%
SR Jenkins Ft Lupton	CO	1.39	13	0.3095	0.3181	0.3078	0.2981	1.3%	-2.3%	-6.7%	-1.7%	-5.4%	-10.4%
Sadiebrook NC Solar	NC	1.34	5	0.2861	0.2932	0.2770	0.2680	0.5%	-0.4%	-4.8%	-2.1%	-2.7%	-7.7%
Sadler Solar	VA	1.28	100	0.2628	0.2715	0.2607	0.2487	0.1%	-1.2%	-3.0%	-1.4%	-3.0%	-4.9%

Table 11: Selected solar sites for the study *with* TMY *and* HIST *production as well as* SIM-YYYY *production percentage differences from* HIST

Solar Site	State	DC/AC	MW	TMY	HIST P10	HIST P50	HIST P90	SIM-2022 P10	SIM-2022 P50	SIM-2022 P90	SIM-2034 P10	SIM-2034 P50	SIM-2034 P90
Sage Solar I-III	UT	1.32	58	0.2840	0.3008	0.2801	0.2674	4.0%	3.9%	-0.7%	5.6%	5.9%	0.9%
Scott Solar Farm	VA	1.35	17	0.2793	0.2811	0.2738	0.2569	0.5%	-2.0%	-2.0%	-1.2%	-3.8%	-4.0%
Scottsburg Solar Park	IN	1.37	7	0.2637	0.2788	0.2615	0.2472	-3.6%	-4.9%	-7.8%	-9.6%	-11.2%	-14.7%
Selmer Farm LLC	TN	1.27	16	0.2651	0.2737	0.2630	0.2484	-0.6%	-4.7%	-8.2%	-6.6%	-10.5%	-14.2%
Shaw Creek Solar, LLC	SC	1.45	75	0.3065	0.3154	0.3018	0.2899	0.8%	-1.8%	-5.6%	-2.0%	-4.4%	-8.9%
Sigurd Solar LLC	UT	1.40	80	0.3145	0.3262	0.3138	0.3027	2.9%	1.2%	-2.1%	3.6%	1.7%	-1.6%
Springbok Solar Farm 2	CA	1.06	155	0.2941	0.2991	0.2931	0.2869	1.1%	-0.6%	-3.9%	0.0%	-2.0%	-5.5%
Springerville	AZ	1.20	8	0.3064	0.3136	0.3059	0.3005	2.8%	-0.2%	-5.3%	1.9%	-1.7%	-6.8%
St. Joseph Solar	IN	1.27	20	0.2323	0.2512	0.2302	0.2216	-5.6%	-4.9%	-10.0%	-12.7%	-12.3%	-17.4%
Starvation	OR	1.55	10	0.3126	0.3202	0.3097	0.2933	3.3%	1.1%	-0.5%	3.9%	1.4%	0.1%
Statesville Solar	NC	1.24	5	0.2652	0.2754	0.2619	0.2485	-0.6%	-2.4%	-5.0%	-4.0%	-5.6%	-8.4%
Stuttgart Solar	AR	1.55	81	0.3148	0.3260	0.3109	0.2955	-1.1%	-3.6%	-7.7%	-6.6%	-9.7%	-14.1%
Sumrall I Solar Farm	MS	1.42	52	0.2992	0.3126	0.3026	0.2853	-0.4%	-5.3%	-8.8%	-5.7%	-10.7%	-14.4%
Trent River Farm	NC	1.44	5	0.2926	0.3016	0.2887	0.2767	1.0%	-0.3%	-2.8%	-0.5%	-1.8%	-4.3%
Troy Solar	IN	1.29	50	0.2542	0.2707	0.2545	0.2411	-3.2%	-4.5%	-7.5%	-8.8%	-10.7%	-14.3%
Turquoise Nevada, LLC	NV	1.02	60	0.2514	0.2607	0.2496	0.2395	2.0%	1.0%	-2.1%	2.4%	0.8%	-1.8%
Two Creeks Solar	WI	1.42	150	0.2507	0.2646	0.2489	0.2367	-2.9%	-3.4%	-6.3%	-7.9%	-9.0%	-12.0%
Two Mile Desert Project	NC	1.30	16	0.2664	0.2759	0.2644	0.2537	0.7%	-1.0%	-4.0%	-0.8%	-2.8%	-6.1%
Vuelta Solar	MA	1.09	6	0.2029	0.2129	0.2029	0.1918	-0.2%	-1.9%	-3.8%	-2.5%	-4.5%	-6.7%
Wapello Solar LLC	IA	1.28	100	0.2514	0.2624	0.2478	0.2348	-2.3%	-3.7%	-7.2%	-6.6%	-8.7%	-12.6%
Water Strider Solar	VA	1.35	80	0.2777	0.2856	0.2777	0.2615	0.1%	-2.2%	-3.0%	-1.6%	-4.3%	-5.3%
Webster Holdco Solar CSG	MN	1.34	5	0.2552	0.2568	0.2483	0.2380	-0.6%	-2.7%	-5.1%	-4.2%	-6.4%	-8.8%
Western Antelope Blue Sky Ranch A	CA	1.19	20	0.3262	0.3310	0.3267	0.3179	1.9%	-0.3%	-2.7%	1.9%	-0.5%	-3.0%
White River Solar 2	CA	1.31	20	0.3287	0.3347	0.3266	0.3169	3.3%	0.9%	-2.9%	3.5%	1.1%	-2.5%
Whitewright Solar	TX	1.40	10	0.3123	0.3182	0.3048	0.2878	0.3%	-4.3%	-8.7%	-4.6%	-9.0%	-13.9%
Wilmot Energy Center LLC	AZ	1.04	130	0.2818	0.2850	0.2800	0.2698	3.0%	-1.1%	-5.4%	1.3%	-3.4%	-7.3%
Wyandot Solar Farm	OH	1.20	10	0.2215	0.2336	0.2182	0.2068	-3.4%	-3.9%	-6.4%	-9.2%	-9.8%	-12.9%